Aminophosphine Palladium(0) Complex Supported on ZrO_2 Nanoparticles (ZrO_2@$AEPH_2$-PPh_2-Pd(0)) as an Efficient Heterogeneous Catalyst for Suzuki–Miyaura and Heck–Mizoroki Reactions in Green Media

Nasrin Razavi, Batool Akhlaghinia & Roya Jahanshahi

🐎 Springer

🐎 Springer

Springer

CrossMark

Aminophosphine Palladium(0) Complex Supported on ZrO_2 Nanoparticles (ZrO_2@$AEPH_2$-PPh_2-Pd(0)) as an Efficient Heterogeneous Catalyst for Suzuki–Miyaura and Heck–Mizoroki Reactions in Green Media

Nasrin Razavi[1] · Batool Akhlaghinia[1] · Roya Jahanshahi[1]

Abstract A new aminophosphine palladium(0) complex supported on ZrO_2 nanoparticles (ZrO_2@$AEPH_2$-PPh_2-Pd(0)) was successfully synthesized and characterized using FT-IR, XRD, XPS, SEM, TEM, EDS, TGA and ICP techniques. Characterization results revealed that the synthesized catalyst had tetragonal and monoclinic structure with spherical morphology. The prepared nanocatalyst was showed excellent reactivity in the Suzuki–Miyaura and Heck–Mizoroki cross-coupling reactions. Moreover, this nanocatalyst can be easily recovered and reused for at least six cycles without deterioration in catalytic activity.

Graphical Abstract

Aminophosphine palladium(0) complex supported on ZrO_2 nanoparticles (ZrO_2@$AEPH_2$-PPh_2-Pd(0)) as an efficient heterogeneous catalyst for Suzuki–Miyaura and Heck–Mizoroki reactions in green media
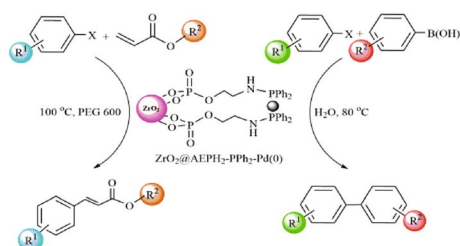

Nasrin Razavi, Batool Akhlaghinia,* Roya Jahanshahi

1. Reusable nanocatalyst was prepared and characterized.
2. ZrO_2@$AEPH_2$-PPh_2-Pd was applied as a novel heterogeneous nanocatalyst for Suzuki–Miyaura and Heck–Mizoroki reactions.

✉ Batool Akhlaghinia
akhlaghinia@um.ac.ir

[1] Department of Chemistry, Faculty of Sciences, Ferdowsi University of Mashhad, 9177948974 Mashhad, Iran

1 Introduction

It is well-known that the carbon–carbon bond formation reactions are among the most fundamental reactions in organic chemistry since the resulting coupling products are widely used as powerful tools in several fields of chemistry

such as pharmaceuticals, agrochemicals and natural products [1–5]. Transition metals or their complexes have been applied as catalyst and promoter in many of these reactions. Among different transition metals [6], palladium-catalyzed cross-coupling reactions have become a very important protocol during the last decades [7–9]. Suzuki–Miyaura [10] and Heck–Mizoroki [11, 12] reactions, which have been recognized as efficient tools and overwhelming favorite topics in advanced organic synthesis for both academic and industrial processes [13, 14], were catalyzed by Pd based catalysts. Generally, traditional Suzuki–Miyaura and Heck–Mizoroki reactions employ the homogeneous palladium catalysts in the presence of various ligands such as phosphines, *N*-heterocyclic carbenes, oxime carbapalladacycle, imidazolium and Schiff bases [15–17]. As some of the homogeneous palladium catalysts have not good results regarding to the coupling of less reactive aryl halides and since Pd-catalysts are expensive and sometimes remain scant contamination in the products, to improve the efficiency and reusability of the catalyst, as well as minimizing the catalyst cost, elaborating of high loading supported Pd-catalysts by immobilizing the Pd-catalysts onto organic and inorganic supporters are much in demand and desirable. Numerous heterogeneous palladium catalysts supported on mesoporous silica [18, 19], proteins [20], carbon nanotubes [21], partially reduced graphene oxide nanosheets [22, 23], NaY zeolites [24], magnetic nanoparticles [25, 26], polymeric microspheres, microcapsules and resins [27–31], were successfully utilized in the Suzuki–Miyaura and Heck–Mizoroki reactions. Although some of these catalytic systems exhibited excellent efficiency, most of them associated with using organic (co)-solvents and/or required high temperatures (above 100 °C) besides high catalyst concentrations (up to 1 mol%) [19, 32]. Additionally, the poor recyclability is another drawback of many of the existing heterogeneous catalysts which is due to the aggregation of nanoparticles into the less reactive large particles (palladium black) owing to the high surface energy of small nanoparticles generated during the catalytic reactions. In this regard, immobilization of ligands or homogeneous catalysts on different types of support materials has been extensively employed to make a recoverable catalytic system [33]. Although, the activity and selectivity of the immobilized catalysts were decreased frequently as a result of the reduction in reactant diffusion rate to the surface of catalyst [34], but this problem can be resolved to some extent by selecting a support possessing the smallest possible size. Thus, nanoparticles are superlative support candidates, wherein, the surface area is increased dramatically due to the nanometer scale.

As the property of a catalytic system strongly depends on the ligand choice [35], tremendous efforts have been dedicated to search for more efficient and affordable ligands. In this respect, improving different aspects of Pd-catalysts is still highly desirable and demanded. Palladium–phosphine and phosphinite complexes are the most intensively investigated catalysts in Heck–Mizoroki and Suzuki–Miyaura coupling reactions regarding to the fact that their catalytic activities can be effectually modulated by the electronic and steric properties of the ligands [14, 36–40].

In recent years, ZrO$_2$ NPs have attracted substantial attention owing to their electrical properties, potential applications in transparent, catalysis, fuel cells, advanced ceramics and sensors [41–44]. Besides the above-mentioned principal applications, ZrO$_2$ NPs have fascinated considerable interest with respect to their feasible applications as a catalyst or catalytic support [45–48]. Isomerization of olefins and epoxides [49], dehydration of alcohols [50], selective synthesis of dimethyl carbonate [51], methanolselective oxidation [52], and redox processes [53], are some of the reactions have been improved by using ZrO$_2$-based NPs.

To date, a few palladium complexes on functionalized ZrO$_2$ NPs have been synthesized and used in the Suzuki–Miyaura and Heck–Mizoroki coupling reactions [54, 55]. Herein, to obtain a stable, low cost and efficient palladium heterogeneous nanocatalyst, we have synthesized a new aminophosphine palladium complex supported on ZrO$_2$ NPs. For this aim, the prepared ZrO$_2$ NPs by sol–gel method [56], was first functionalized by 2-aminoethyl dihydrogen phosphate (AEPH$_2$) through the phosphate groups [57], which afforded ZrO$_2$@AEPH$_2$. Subsequently, the reaction of ZrO$_2$@AEPH$_2$ with ClPPh$_2$ in the presence of Et$_3$N at room temperature, produced ZrO$_2$@AEPH$_2$-PPh$_2$ which was next used as a great support for entrapment of Pd by treating with Pd(OAc)$_2$ in methanol (Scheme 1).

The superior catalytic activity of ZrO$_2$@AEPH$_2$-PPh$_2$-Pd(0) as a new heterogeneous nanocatalyst was proved towards the Suzuki–Miyaura and Heck–Mizoroki coupling reactions, in green media (see Scheme 2 and 3).

2 Experimental

### 2.1 Materials

All chemical reagents and solvents were purchased from Merck and Sigma-Aldrich chemical companies and were used as received without further purification. ZrO$_2$ NPs were prepared by the previously reported method in literature [56].
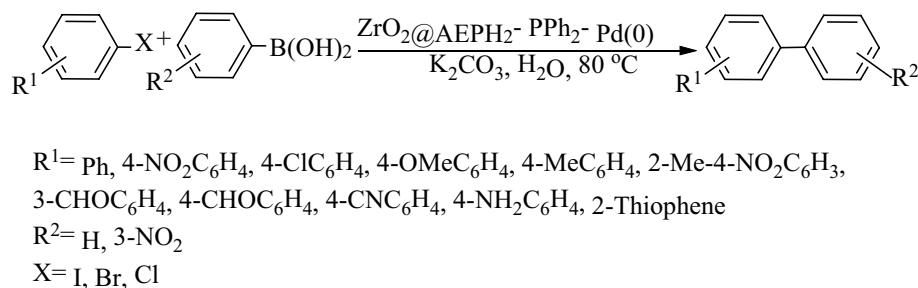
2.2 Instrumentation Analysis

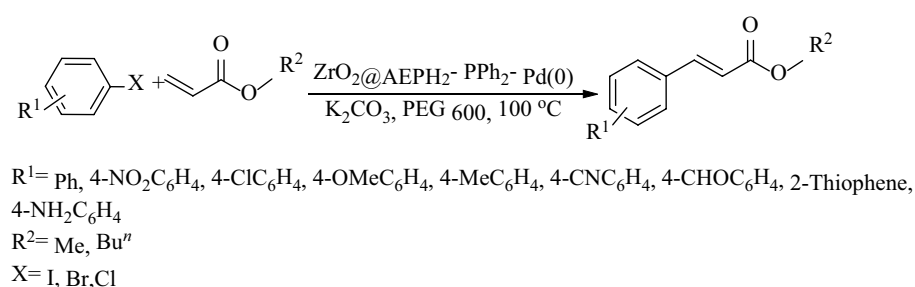The purity determinations of the products and the progress of the reactions were accomplished by TLC on silica gel

Scheme 1 Preparation steps of ZrO$_2$@AEPH$_2$-PPh$_2$-Pd(0) nanocatalyst
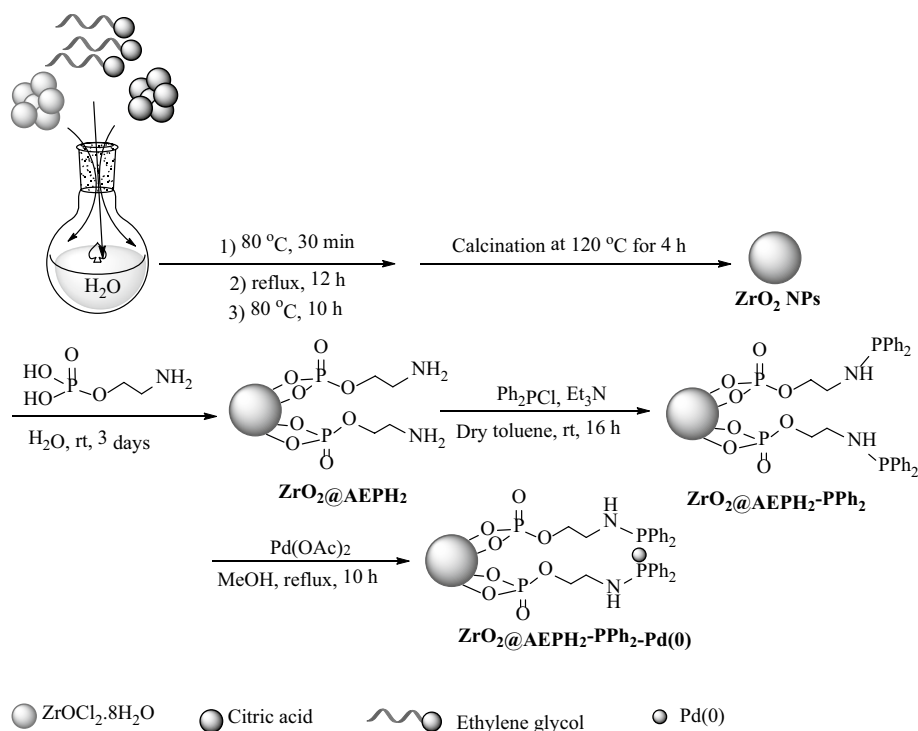
Scheme 2 Suzuki–Miyaura coupling reaction in the presence of ZrO$_2$@AEPH$_2$-PPh$_2$-Pd(0) nanocatalyst

R^1= Ph, 4-NO$_2$C$_6$H$_4$, 4-ClC$_6$H$_4$, 4-OMeC$_6$H$_4$, 4-MeC$_6$H$_4$, 2-Me-4-NO$_2$C$_6$H$_3$, 3-CHOC$_6$H$_4$, 4-CHOC$_6$H$_4$, 4-CNC$_6$H$_4$, 4-NH$_2$C$_6$H$_4$, 2-Thiophene
R^2= H, 3-NO$_2$
X= I, Br, Cl

Scheme 3 Heck–Mizoroki coupling reaction in the presence of ZrO$_2$@AEPH$_2$-PPh$_2$-Pd(0) nanocatalyst

R^1= Ph, 4-NO$_2$C$_6$H$_4$, 4-ClC$_6$H$_4$, 4-OMeC$_6$H$_4$, 4-MeC$_6$H$_4$, 4-CNC$_6$H$_4$, 4-CHOC$_6$H$_4$, 2-Thiophene, 4-NH$_2$C$_6$H$_4$
R^2= Me, Bu^n
X= I, Br,Cl

polygram STL G/UV 254 plates. The melting points of products were determined with an Electrothermal Type 9100 melting point apparatus. The FT-IR spectra were recorded on pressed KBr pellets using AVATAR 370 FT-IR spectrometer (Therma Nicolet spectrometer, USA) at room temperature in the range between 4000 and 400 cm^{-1} with a resolution of 4 cm^{-1}. The NMR spectra were provided on Brucker Avance 300, 400 and 500 MHz instruments in DMSO-d_6 and CDCl$_3$. Mass spectra were recorded with a CH7A Varianmat Bremem instrument at 70 eV electron impact ionization, in *m/z* (rel %). TGA analysis was performed using a Shimadzu Thermogavimetric Analyzer (TG-50) in the temperature range of 25–800 °C at a heating rate of 10 °C min^{-1} under air atmosphere. SEM images

were recorded using Leo 1450 VP (LEO, Germany) scanning electron microscope operating at an acceleration voltage 20 kV, resolution of about 2 nm. Transmission electron microscopy (TEM) was performed with a Leo 912 AB microscope (Zeiss, Germany) with an accelerating voltage of 120 kV. The crystal structure of catalyst was analyzed by XRD using a D8 ADVANCE–Bruker diffractometer operated at 40 kV and 30 mA utilizing Cu$K\alpha$ radiation ($\lambda = 0.154$ Å). Surface analysis spectroscopy of the catalyst was performed in an ESCA/AES system. This system was equipped with a concentric hemispherical (CHA) electron energy analyzer (Specs model EA10 plus) suitable for X-ray photoelectron spectroscopy (XPS). Inductively coupled plasma (ICP) analysis was carried out with a Varian VISTA-PRO, CCD (Australia). The content of metal leached in the recovered solutions after catalysis was determined by inductively coupled plasma optical emission spectrometer (ICP-OES) analyzer (Spectro Arcos, Germany). All yields refer to isolated products after purification by thin layer chromatography. In addition, all of the products were known compounds and they were characterized by ^{1}H NMR, ^{13}C NMR spectroscopy, and mass spectrometry and comparison of their melting points with known compounds (see supporting information).

2.3 Preparation of ZrO$_2$ NPs

To a solution of ZrOCl$_2$.8H$_2$O (0.003 mol, 0.966 g) in 50 mL distilled water, citric acid (0.126 mol, 24.207 g) and ethylene glycol (0.126 mol, 7.045 mL) were added, at room temperature. The resulting solution was stirred at 80 °C for 30 min, followed by refluxing for 12 h until a white sol was obtained. In order to increase polymerization between citric acid, ethylene glycol, and ZrOCl$_2$.8H$_2$O, the reaction mixture was cooled down and then slowly heated at 80 °C for 10 h in an open bath. Afterwards, the sol became more viscous as a wet gel. Finally, the wet gel was dried by direct heating on the hot plate at 120 °C for 8 h to afford a brown powder. The powder was calcined at 750 °C for 4 h at a rate of 4 °C min, to give ZrO$_2$ NPs as a white powder [56].

2.4 Preparation of ZrO$_2$@AEPH$_2$

ZrO$_2$ NPs (1 g) were sonicated in distilled water (5 mL), for 30 min. A solution of AEPH$_2$ (5 mmol, 0.7 g) in methanol (15 mL) was then added to the above aqueous particle dispersion. Thereafter, HCl solution (0.028 M) was added drop by drop into the mixture, under vigorous stirring at room temperature. When pH was adjusted to 2.0, addition of HCl solution was stopped. The resulting suspension was stirred at room temperature for 3 days. At the end, the precipitate was separated by centrifugation (10,000 rpm for

15 min) and washed with distilled water (5 × 15 mL) before being dried under vacuum at 100 °C for 16 h [57].

2.5 Preparation of ZrO$_2$@AEPH$_2$-PPh$_2$

ZrO$_2$@AEPH$_2$ (1 g) and Et$_3$N (3 mL) were dispersed in dry toluene (50 mL), under ultrasonication, for 30 min. Next, chlorodiphenylphosphine (5 mL) was slowly dropped into the above mixture and the suspension was stirred magnetically for 16 h at room temperature. Finally, the suspension was centrifuged at 10,000 rpm for 15 min and the obtained residue was washed with ethanol (5 × 10 mL), followed by drying under vacuum at 80 °C for 16 h to afford ZrO$_2$@AEPH$_2$-PPh$_2$ as a white powder.

2.6 Preparation of ZrO$_2$@AEPH$_2$-PPh$_2$-Pd(0)

ZrO$_2$@AEPH$_2$-PPh$_2$ (2 g) was added to a mixture of Pd(OAc)$_2$ (0.34 mmol, 0.076 g) in methanol (10 mL). The reaction mixture was refluxed for 10 h. After that, the resultant mixture was cooled and the precipitate was separated by centrifugation. Thereupon, the obtained nano particles were washed with methanol (5 × 10 mL), to remove any free metal species followed by drying in a vacuum oven at 100 °C for 24 h.

2.7 Typical Procedure for Suzuki–Miyaura Coupling Reaction

Potassium carbonate (1.5 mmol, 0.207 g) was added to a mixture of iodobenzene (1.0 mmol, 0.203 g) and phenylboronic acid (1.2 mmol, 0.146 g), in water (3 mL) at 80 °C. Then, to the resulting mixture ZrO$_2$@AEPH$_2$-PPh$_2$-Pd(0) (0.2 mol%, 0.004 g) was added under stirring. After the completion of the reaction (20 min) which was monitored by TLC, the nanocatalyst was recovered by centrifugation, washed with ethyl acetate and dried under vacuum at 100 °C for 24 h. The reaction mixture was then extracted with ethyl acetate (5 × 5 mL) and the combined organic layer was dried over anhydrous Na$_2$SO$_4$. After evaporation of the solvent, the crude product was purified by thin layer chromatography using n-hexane/ethyl acetate (50/1) to afford the pure product (0.145 g, % 95 yield).

2.8 Typical Procedure for Heck–Mizoroki Coupling Reaction

Potassium carbonate (1.5 mmol, 0.207 g) was added to a mixture of iodobenzene (1.0 mmol, 0.203 g) and methyl acrylate (1.2 mmol, 0.108 mL), in PEG 600 (3 mL) at 100 °C. Then, to the resulting mixture ZrO$_2$@AEPH$_2$-PPh$_2$-Pd(0) (0.2 mol%, 0.004 g) was added under stirring. After the completion of the reaction (30 min) which was

monitored by TLC, the nanocatalyst was recovered by centrifugation, washed with ethyl acetate and dried under vacuum at 100 °C for 24 h. The reaction mixture was then extracted with ethyl acetate (5×5 mL) and the combined organic layer was dried over anhydrous Na_2SO_4. After evaporation of the solvent, the crude product was purified by thin layer chromatography using *n*-hexane/ethyl acetate (50/1) to afford the pure product (0.153 g, % 95 yield).

3 Results and Discussion

3.1 Characterization of ZrO_2@$AEPH_2$-PPh_2-Pd(0) Nanocatalyst

The chemical structure and morphology of the as-synthesised nanocatalyst was determined by various techniques, such as Fourier transform infrared spectroscopy (FT-IR), X-ray powder diffraction (XRD), X-ray photoelectron spectroscopy (XPS), scanning electron microscopy (SEM), transmission electron microscopy (TEM), energy dispersive spectrum (EDS), thermogravimetric analysis (TGA) and inductively coupled plasma (ICP).

FT-IR spectra of ZrO_2 NPs, ZrO_2@$AEPH_2$, ZrO_2@$AEPH_2$-PPh_2, and ZrO_2@$AEPH_2$-PPh_2-Pd(0) were shown in Fig. 1. In FT-IR spectrum of ZrO_2 NPs (Fig. 1a), a broad absorption band at around 3450–3200 cm^{-1} was attributed to the asymmetric and symmetric stretching vibrations of hydroxyl groups in the structure of ZrO_2 NPs and also hydroxyl groups of residual water in ZrO_2 NPs framework. The strong absorption bands at 751 and 507 cm^{-1} were referred to the stretching vibrations of Zr–O groups in ZrO_2 NPs. Upon functionalization of ZrO_2 NPs with $AEPH_2$, the intensity of the absorption band at 3500–2900 cm^{-1} was increased due to the presence of NH_2 groups (Fig. 1b). Also, the absorption bands observed at 1151 and 1035 cm^{-1} could be assigned to the stretching vibrations of P=O and Zr–O–P, respectively, which confirmed the prosperous chemical attachment of $AEPH_2$ to the surface of ZrO_2 NPs. On the other hand, the symmetric stretching and bending vibrations of O–P–O bonds at 1099, 981 and 570–604 cm^{-1} were covered by the broad absorption band of Zr–O at around 746–416 cm^{-1}. As shown in Fig. 1c, the absorption band at around 3060 cm^{-1} was attributed to the C–H stretching vibration of the phenyl ring in the structure of ZrO_2@$AEPH_2$-PPh_2. Besides, the weak absorption band at 1437 cm^{-1} was ascribed to the stretching vibration of P–C bond. The strong absorption band at 1130–1090 cm^{-1} relating to the P-phenyl stretching vibrations, increased the intensity of the absorption bands of P=O and Zr–O–P vibrations around 1217–1070 cm^{-1}. However, FT-IR spectrum of ZrO_2@$AEPH_2$-PPh_2-Pd(0)
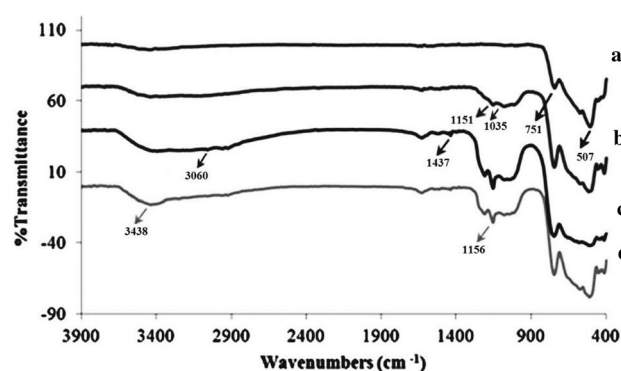

Fig. 1 FT-IR spectra of *a* ZrO_2 NPs, *b* ZrO_2@$AEPH_2$, *c* ZrO_2@ $AEPH_2$-PPh_2 and *d* ZrO_2@$AEPH_2$-PPh_2-Pd(0)

(Fig. 1d) considerably confirmed the coordination of Pd, by decreasing the intensity of P-phenyl stretching vibrations at around 1217–1070 cm^{-1}. Even though the FT-IR spectrum of ZrO_2@$AEPH_2$-PPh_2-Pd(0) did not show noticeable changes after immobilization of palladium on the ZrO_2@$AEPH_2$-PPh_2 surface [58], but the XRD pattern of ZrO_2@$AEPH_2$-PPh_2-Pd(0) nanocatalyst clearly evidenced the presence of Pd on the surface of the functionalized ZrO_2 NPs.

Figure 2 shows the XRD diffraction patterns of the prepared ZrO_2 NPs, ZrO_2@$AEPH_2$-PPh_2-Pd(0) and sixth reused of ZrO_2@$AEPH_2$-PPh_2-Pd(0) nanocatalyst. As can be seen in Fig. 2a, the synthesized ZrO_2 NPs are a mixture of monoclinic and tetragonal phases corresponding to JCPDS files no. 37-1484 and 79-1771, respectively [59, 60]. The ratio of these two phases is difficult to determine. In the XRD pattern of ZrO_2@$AEPH_2$-PPh_2-Pd(0) (Fig. 2b), the main peaks relating to ZrO_2 NPs could be seen. In this pattern, the peak positions of ZrO_2 NPs were not changed during the synthesis of ZrO_2@$AEPH_2$-PPh_2-Pd(0). This result means that the ZrO_2@$AEPH_2$-PPh_2-pd(0) nanocatalyst has been synthesized successfully without damaging the crystal structure of ZrO_2 NPs. Also, two weak peaks appeared at $2\theta = 40.1$ and 46.5 could be related to the existence of Pd(0) [61]. The Pd peaks of ZrO_2@$AEPH_2$-PPh_2-Pd(0) nanocatalyst agree well with the standard Pd (cubic phase) XRD spectrum (card No. 05-0681). According to the XRD pattern of ZrO_2@$AEPH_2$-PPh_2-Pd(0), the intensity of the new peaks attesting the presence of Pd is weak which may be attributed to the good dispersion of Pd nanoparticles in the catalysis matrix. So, Pd nanoparticles cannot lead to the formation of regular crystal lattice [55]. The active Pd(0) catalyst required for these reactions, was typically created by the coordination of two P atoms to a Pd(II) center, which subsequently reduced Pd(II) to Pd(0) *via* an additional phosphinite moiety [62–66]. On the other hand, Pd immobilization on the surface of modified ZrO_2 were
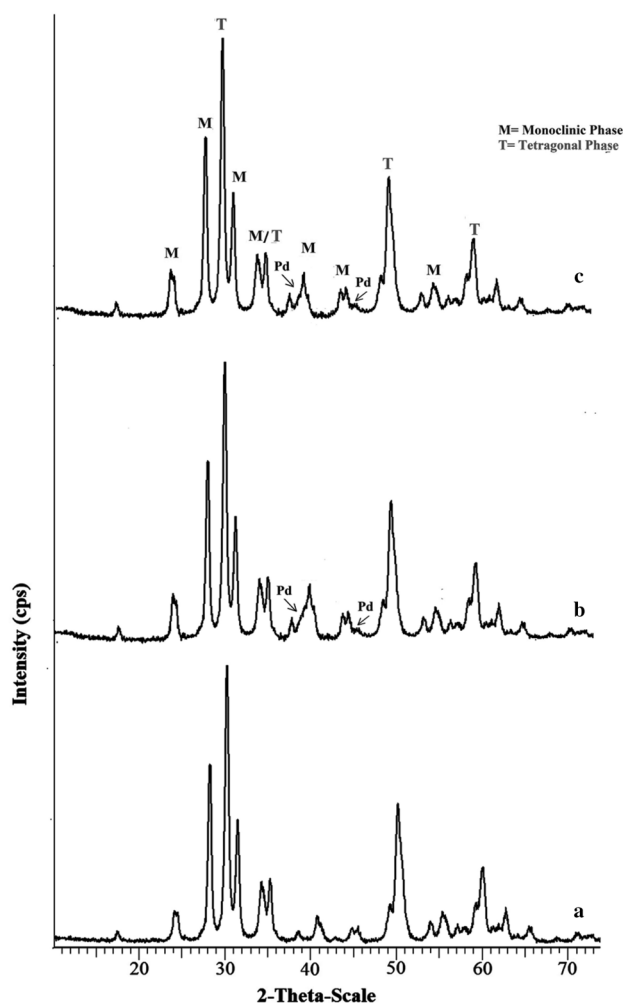
Fig. 2 XRD patterns of *a* ZrO₂ NPs, *b* ZrO₂@AEPH₂-PPh₂-Pd(0) and *c* sixth reused of ZrO₂@AEPH₂-PPh₂-Pd(0)

Fig. 3 a XPS spectra of fresh catalyst and **b** sixth reused of ZrO₂@AEPH₂-PPh₂-Pd(0)

took place in methanol media, which is a known reducing agent in Pd(0) formation [67–69].

In order to get some information about the oxidation state and the electron environment of palladium immobilized on the surface of ZrO₂ NPs, X-ray photoelectron spectra (XPS) of the fresh ZrO₂@AEPH₂-PPh₂-Pd(0) nanocatalyst and the sixth reused nanocatalyst were studied (Fig. 3). Although, there was an overlapping between the dominant photoelectron peaks of Pd ($3d_{3/2}$ (340.4 eV) and $3d_{5/2}$ (335.1 eV) and the zirconium 3p core level peaks $3p_{1/2}$ (~346.6 eV) and $3p_{3/2}$ (~332.9 eV) in ZrO₂ [70], two weak peaks at 335.5 eV (Pd(0) $3d_{5/2}$) and 340.8 eV (Pd(0) $3d_{3/2}$) were observed, which clearly indicates that the Pd nanoparticles are stable as metallic state in the nanocatalyst structure (Fig. 3a). In comparison with the standard binding energy of Pd(0), there was a shift in the binding energy values and this must be due to interaction of Pd(0) with phosphorous atoms of chlorodiphenylphosphine [65].
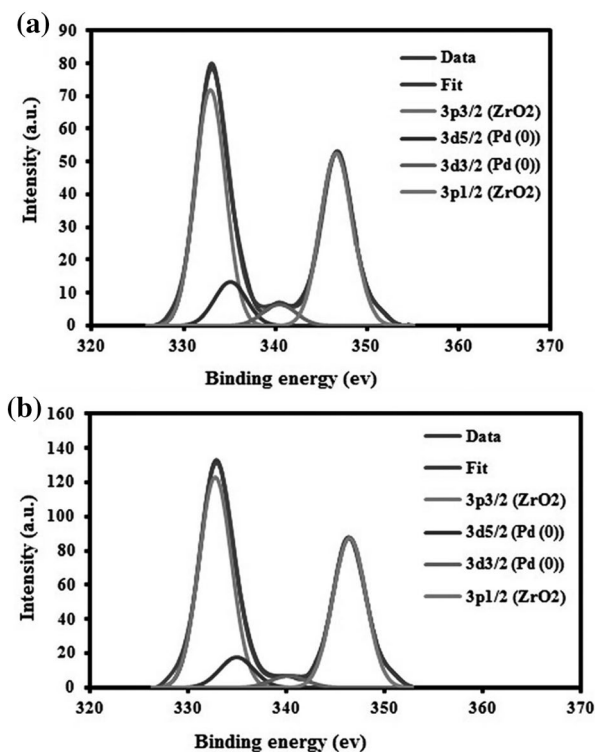
Surface morphology and size of the as-synthesized nanocatalyst, which are the important factors affecting the catalytic performance, were investigated by scanning electron microscopy (SEM) and transmission electron microscopy (TEM). Figure 4a, b represents the SEM images of the ZrO₂@AEPH₂-PPh₂-Pd(0) nanocatalyst. These images illustrate that the functionalized ZrO₂ NPs have spherical morphology. Moreover, it could be deduced that the surface of nanocatalyst is not smooth and composed of many tiny particles. The TEM images of the nanocatalyst (Fig. 4e, f) depicted the presence of spherical particles with an average size ranging of 10–40 nm.

The energy dispersive spectrum (EDS) indicated the presence of C, O, Zr and Pd elements (Fig. 5). This analysis confirmed that Pd is successfully supported on ZrO₂@AEPH₂-PPh₂ nanocatalyst.

Thermogravimetric analysis (TGA) of ZrO₂@AEPH₂-PPh₂-Pd(0) was carried out to investigate the thermal stability and content of organic functional groups on the surface of nanocatalyst (Fig. 6). It is evidently obvious that the thermogravimetric diagram exhibited a weight loss of about 5% at temperatures below 200 °C corresponding to the removal of physically adsorbed water on the catalyst surface. The second weight loss at 200–800 °C (13%), is relating to the decomposition of AEPH₂ and PPh₂ groups grafted onto the ZrO₂ NPs surface. According to the

Fig. 4 SEM images of $ZrO_2@$ $AEPH_2$-PPh_2-Pd(0) (**a, b**), sixth reused $ZrO_2@AEPH_2$-PPh_2-Pd (0) (**c, d**) and TEM images of $ZrO_2@AEPH_2$-PPh_2-Pd(0) (**e, f**), sixth reused $ZrO_2@AEPH_2$- PPh_2-Pd(0) (**g, h**)
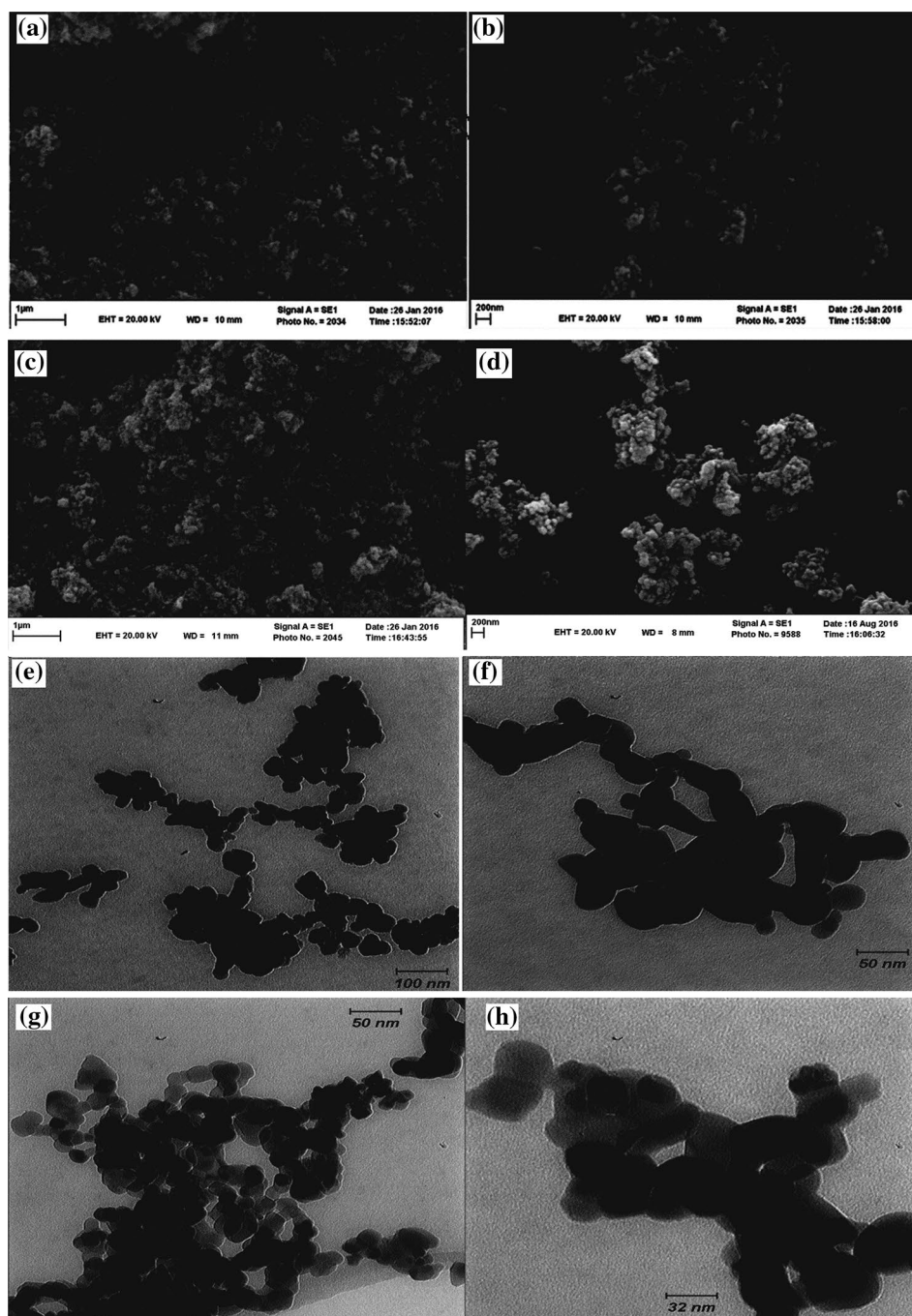
TGA thermogram, it can be estimated that the amount of $AEPH_2$-PPh_2 supported on the surface of catalyst is about 0.45 mmol g^{-1}. Also, from the TGA, it can be verified that the presented nanocatalyst has a great thermal stability.

In addition, the exact amount of Pd on the surface of $ZrO_2@AEPH_2$-PPh_2 nanocatalyst was determined by inductively coupled plasma (ICP) analysis. Accordingly, the loading amount of Pd on the $ZrO_2@AEPH_2$-PPh_2 nano-catalyst was found to be about 0.43 mmol g^{-1}.

3.2 Catalytic Activity of $ZrO_2@AEPH_2$-PPh_2-Pd(0) in Suzuki–Miyaura and Heck–Mizoroki Coupling Reactions

After the successful preparation and full characterization of $ZrO_2@AEPH_2$-PPh_2-Pd(0), in continuation of our recent efforts to investigate the applications of heterogeneous catalysts in organic transformations [71–78], the catalytic performance of $ZrO_2@AEPH_2$-PPh_2-Pd(0) as a new reusable

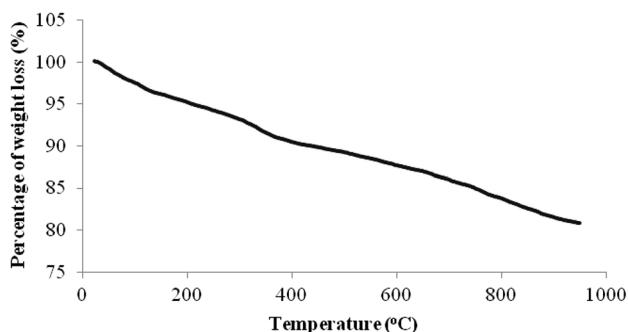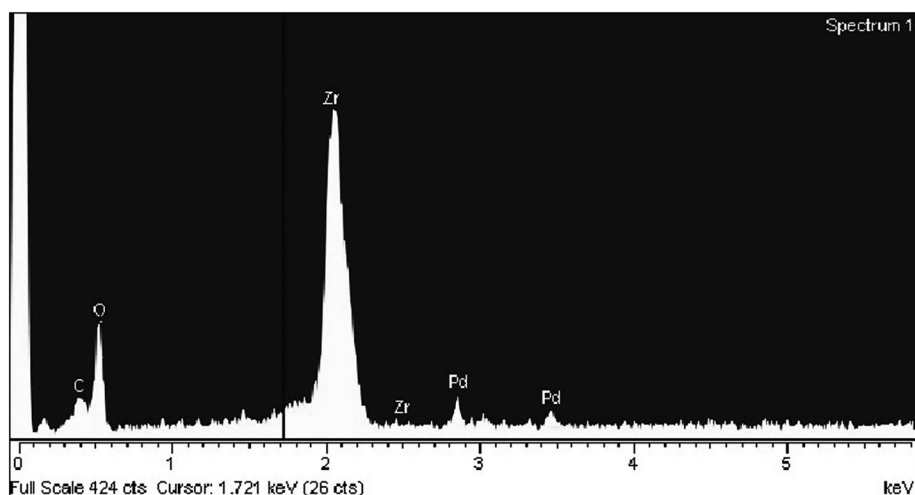**Fig. 5** EDS spectrum of ZrO$_2$@AEPH$_2$-PPh$_2$-Pd (0)

Fig. 6 TGA thermogram of ZrO$_2$@AEPH$_2$-PPh$_2$-Pd(0) nanocatalyst

nanocatalyst was evaluated for Suzuki–Miyaura coupling reaction (Scheme 2).

In order to find the optimal reaction conditions for such a transformation, the reaction of iodobenzene (1 mmol) with phenylboronic acid (1.2 mmol) was chosen as a test model for optimizing the reaction parameters including different solvents, temperatures, bases and amount of catalyst (Table 1). Initially, the model reaction was performed in DMF as solvent by applying 1:2 molar ratio of iodobenzene/base, under catalyst-free conditions at 100 °C. With regard to the results in Table 1, it was observed that the reaction progress was not satisfactorily even after a prolonged reaction time (24 h), and the achieved product yield was only 10% (Table 1, entry 1).

However, using 0.2 mol% of ZrO$_2$@AEPH$_2$-PPh$_2$-Pd(0) nanocatalyst in Suzuki–Miyaura reaction, furnished the corresponding product in excellent yield, within 15 min (Table 1, entry 2). Solvent screening was also performed to examine the effect of various solvents on this reaction (Table 1, entries 2–7). The experimental results exhibited that the excellent yield (95%) of the product was obtained

in DMF and H$_2$O. Nevertheless, owing to safety, economic and handling considerations, H$_2$O was chosen as the optimum choice of solvent for further experiments. In the next stage, the influence of variety of bases such as K$_2$CO$_3$, Et$_3$N, NaOAc, *N,N*-diisopropyl amine, NaHCO$_3$ and Na$_2$CO$_3$ on the progress of the reaction, was investigated (Table 1, entries 7–12). Among the tested bases, the low-cost K$_2$CO$_3$ was clearly stood out as the best choice, with respect to the reaction time (15 min) and product yield (95%). During our optimization studies, the progress of Suzuki–Miyaura reaction in different temperatures in H$_2$O, was also examined (Table 1, entries 7 and 13–15). As can be seen in Table 1, decreasing the reaction temperature to 80 °C did not have any considerable effect on the reaction progress, whereas, further temperature decreasing (to 60 °C) diminished the reaction rate, significantly. After selecting K$_2$CO$_3$ as the optimal base, we investigated the influence of molar ratios of iodobenzene/base in Suzuki–Miyaura reaction (Table 1, entries 14, 16 and 17). Although, reducing the molar ratio of iodobenzene/base from 1:2 to 1:1.5 was found to have no effect on the product yield (95%), but the desired product was obtained in lower yield (85%), using 1:1.2 molar ratio of iodobenzene/base. It is clearly observed that under the presented reaction conditions when the reaction was performed in the presence of fewer amount of catalyst, lower yield of product was acquired within longer reaction time. In contrast, a further enhancement in the amount of catalyst did not improve the product yield any more (Table 1, entries 16, 18 and 19).

In order to establish the generality and versatility of the present methodology, synthesis of a variety of biphenyl coupled products was studied under the optimized reaction conditions (Table 1, entry 16). The results were presented in Table 2. As shown in Table 2, a range of aryl iodides reacted with phenylboronic acid/or 3-nitro phenylboronic acid, to produce the corresponding products in

Table 1 The Suzuki–Miyaura reaction of iodobenzene with phenylboronic acid in the presence of ZrO$_2$@AEPH$_2$-PPh$_2$-Pd(0) nanocatalyst under different reaction conditions[a]

| Entry	Catalyst (mol%)	Molar ratios of iodobenzene /base	Temperature (°C)	Base	Solvent	Time (min)	Isolated yield (%)
1	–	1/2	100	K$_2$CO$_3$	DMF	24 h	10
2	0.2	1/2	100	K$_2$CO$_3$	DMF	15	95
3	0.2	1/2	100	K$_2$CO$_3$	EtOH	15	85
4	0.2	1/2	100	K$_2$CO$_3$	CH$_3$CN	120	40
5	0.2	1/2	100	K$_2$CO$_3$	Toluene	24 h	20
6	0.2	1/2	100	K$_2$CO$_3$	1,4-Dioxane	24 h	30
7	0.2	1/2	100	K$_2$CO$_3$	H$_2$O	15	95
8	0.2	1/2	100	Et$_3$N	H$_2$O	15	90
9	0.2	1/2	100	NaOAc	H$_2$O	120	50
10	0.2	1/2	100	N,N-diisopropyl amine	H$_2$O	15	90
11	0.2	1/2	100	NaHCO$_3$	H$_2$O	15	80
12	0.2	1/2	100	Na$_2$CO$_3$	H$_2$O	15	90
13	0.2	1/2	90	K$_2$CO$_3$	H$_2$O	20	95
14	0.2	1/2	80	K$_2$CO$_3$	H$_2$O	20	95
15	0.2	1/2	60	K$_2$CO$_3$	H$_2$O	60	80
16	**0.2**	**1/1.5**	**80**	**K$_2$CO$_3$**	**H$_2$O**	**20**	**95**
17	0.2	1/1.2	80	K$_2$CO$_3$	H$_2$O	20	85
18	0.1	1/1.5	80	K$_2$CO$_3$	H$_2$O	30	80
19	0.3	1/1.5	80	K$_2$CO$_3$	H$_2$O	20	95

Bold indicates the optimized reaction conditions

[a]Reaction conditions: iodobenzene (1 mmol), phenylboronic acid (1.2 mmol)

high yields. Among the various tested aryl iodides, those functionalized with electron-withdrawing substituents delivered excellent yields of product, while aryl iodides bearing electron-releasing substituents such as –OCH$_3$ and CH$_3$ at *para* position, required more reaction time to proceed properly (Table 2. entries 2, 3 vs. entries 4, 5). Also, in the case of the sterically hindered substrate, satisfactory yield was obtained in reasonable time (Table 2, entry 6). This new catalytic system was also successfully applied for the coupling reaction of iodo heterocyclic compounds (2-iodothiophene) with phenylboronic acid to afford 90% of the corresponding product within 60 min (Table 2, entry 7). In the same way, the reaction of iodobenzene and 4-methoxy-iodobenzene with 3-nitrophenylboronic acid were examined. In these cases, the desired products were obtained in promising yields, although longer reaction times were required (Table 2, entries 8, 9). To extend the scope of the present study, we next investigated the coupling reaction of various aryl bromides with phenylboronic acid. In comparison with aryl iodides, the reactions of boromo derivatives led to reasonable yields of products, albeit the prolonged reaction times were necessary to complete the reactions (Table 2, entries 10–16). Furthermore, we have examined the reactivity of aryl chlorides such as chlorobenzene, 4-chlorobenzaldehyde and 4-chloroaniline

in the Suzuki–Miyaura coupling reaction. It was observed that the poor yields of the products were obtained, that might be ascribed to the strong strength of the C–Cl bond, which has a 96 kcal/mol bond dissociation energy (Table 2, entries 17–19).

Encouraged by the outstanding catalytic activity of the ZrO$_2$@AEPH$_2$-PPh$_2$-Pd(0) nanocatalyst obtained in the Suzuki–Miyaura reaction, the effectiveness of this new catalyst was also probed in the Heck-Mizoroki reaction (Scheme 3). Along this line, the model reaction of iodobenzene (1 mmol) with methyl acrylate (1.2 mmol) was performed under the optimum reaction conditions relating to Suzuki–Miyaura reaction (Table 1, entry 16). Results showed that the product yield is very negligible even after long period of time (Table 3, entry 1). In an effort to develop better reaction conditions, different solvents such as EtOH, DMF, PEG 600, toluene, 1,4-dioxane and glycerol besides the solvent-free conditions were screened for this transformation, in the presence of 0.2 mol% of ZrO$_2$@AEPH$_2$-PPh$_2$-Pd(0) (Table 3, entries 2–8). As is evident from Table 3, when the reaction was performed in EtOH, toluene, and 1,4-dioxane, the desired product obtained in low yield but DMF and glycerol slightly gave higher yields. As shown, the best result was achieved by carrying out the reaction in PEG 600 as a

Table 2 Suzuki–Miyaura cross-coupling reactions of aryl iodides/bromides with arylboronic acids catalyzed by ZrO$_2$@AEPH$_2$-PPh$_2$-Pd(0)
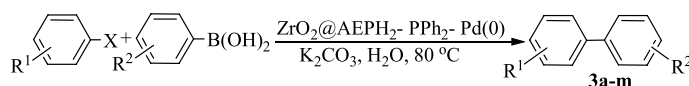
Entry	R^1	R^2	X	Product	Time (min)	Isolated yield (%)
1	H	H	I	3a	20	95
2	4-NO$_2$	H	I	3b	30	95
3	4-Cl	H	I	3c	30	92
4	4-OMe	H	I	3d	60	90
5	4-Me	H	I	3e	45	90
6	2-Me-4-NO$_2$	H	I	3f	30	85
7	2-Thiophene	H	I	3g	60	90
8	H	3-NO$_2$	I	3h	45	85
9	4-OMe	3-NO$_2$	I	3i	60	80
10	H	H	Br	3a	30	90
11	4-NO$_2$	H	Br	3b	45	95
12	4-Cl	H	Br	3c	45	90
13	4-CN	H	Br	3j	45	92
14	4-CHO	H	Br	3k	45	90
15	3-CHO	H	Br	3l	60	90
16	4-OMe	H	Br	3d	180	70
17	H	H	Cl	3a	3 h/24 h	30/30
18	4-CHO	H	Cl	3k	5 h/24 h	45/45
19	4-NH$_2$	H	Cl	3m	5 h/24 h	trace/trace

Table 3 Heck–Mizoroki coupling reaction of iodobenzene with methyl acrylate in the presence of ZrO$_2$@AEPH$_2$-PPh$_2$-Pd(0) under different reaction conditions[a]

Entry	Catalyst (mol%)	Molar ratios of iodobenzene/base	Temperature (°C)	Base	Solvent	Time (min)	Isolated yield (%)
1	0.2	1/1.5	80	K$_2$CO$_3$	H$_2$O	5 h	10
2	0.2	1/1.5	80	K$_2$CO$_3$	EtOH	5 h	30
3	0.2	1/1.5	80	K$_2$CO$_3$	DMF	30	85
4	0.2	1/1.5	80	K$_2$CO$_3$	PEG 600	30	90
5	0.2	1/1.5	80	K$_2$CO$_3$	Toluene	5 h	10
6	0.2	1/1.5	80	K$_2$CO$_3$	1,4-Dioxane	5 h	40
7	0.2	1/1.5	80	K$_2$CO$_3$	Glycerol	30	80
8	0.2	1/1.5	80	K$_2$CO$_3$	–	5 h	10
9	0.2	1/1.5	90	K$_2$CO$_3$	PEG 600	30	92
10	**0.2**	1/1.5	**100**	**K$_2$CO$_3$**	**PEG 600**	**30**	**95**
11	0.2	1/1.5	110	K$_2$CO$_3$	PEG 600	30	95
12	0.2	1/1.5	100	Et$_3$N	PEG 600	30	90
13	0.1	1/1.5	100	K$_2$CO$_3$	PEG 600	30	80
14	0.3	1/1.5	100	K$_2$CO$_3$	PEG 600	30	95
15	–	1/1.5	100	K$_2$CO$_3$	PEG 600	24 h	30

Bold indicates the optimized reaction conditions

[a]Reaction conditions: iodobenzene (1 mmol), methyl acrylate (1.2 mmol)

solvent (Table 3, entry 4). Additionally, in solvent-free conditions, the desired product was obtained in low yield (10%), in an extended reaction time (Table 3, entry 8).

In another experiment, the effect of temperature on the reaction progress was also evaluated and it was found that the reaction proceeded more efficiency by increasing the

temperature up to 100 °C (Table 3, entries 4 and 9–10). Importantly, further increasing of temperature to 110 °C, did not improve the results to any great extent. (Table 3, entry 11). Hence, the optimal temperature for this reaction was chosen to be 100 °C. In the next stage, the effect of organic base on the model reaction was studied. Excitingly, the results revealed that applying inorganic base was more efficient than Et_3N (Table 3, entry 10 vs. entry 12). To study the efficacy of catalyst amount, different amounts of ZrO_2@AEPH$_2$-PPh$_2$-Pd(0) nanocatalyst were also examined in the Heck–Mizoroki coupling reaction. It is obvious from the results that decreasing the amount of catalyst (to 0.1 mol%) led to gain the lower product yield, whilst increasing the catalyst amount (to 0.3 mol%) showed no further increase in the yield of the product (Table 3, entries 13, 14). As observed, a blank experiment in the absence of any catalyst furnished very low yield of the desired product. (Table 3, entry 15).

With these impressive results in hand, in the next step, we have investigated the Heck–Mizoroki reactions of a wide range of aryl halides with methyl and *n*-butyl acrylate

in the presence of ZrO_2@AEPH$_2$-PPh$_2$-Pd(0), under the optimized reaction conditions.

For this purpose, at first, a range of structurally divergent aryl iodides underwent the coupling reaction with methyl acrylate to examine the effect of different substituent on such a reaction. According to the results presented in Table 4, aryl iodides bearing electron-withdrawing groups provided the corresponding products in excellent yields (Table 4, entries 2, 3).

Likewise, aryl iodides containing electron-releasing substituent reacted as well and delivered high yields of the desired products despite the prolonged reaction times (Table 4, entries 4, 5). It is noteworthy that the heterocyclic iodide such as 2-iodothiophene was also a suitable substrate in this protocol and afforded the corresponding product in 83% yield (Table 4, entry 6). Gratifyingly, this catalytic system was also successfully applied for the coupling reactions of substituted aryl bromides. However, as it is clear in Table 4, the reactions of bromo derivatives took a long time to achieve the admissible yields of products, regarding to the less activity of such bromides in comparison with their

Table 4 Heck–Mizoroki cross-coupling reactions of aryl iodides/bromides with olefins catalyzed by ZrO_2@AEPH$_2$-PPh$_2$-Pd(0)
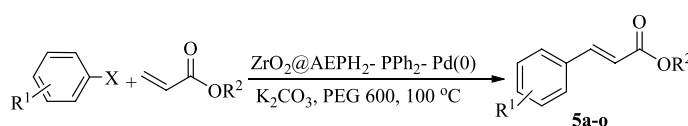
Entry	R^1	R^2	X	Product	Time (min)	Isolated yield (%)
1	H	Me	I	5a	30	95
2	4-NO$_2$	Me	I	5b	20	95
3	4-Cl	Me	I	5c	30	92
4	4-OMe	Me	I	5d	45	85
5	4-Me	Me	I	5e	45	90
6	2-Thiophene	Me	I	5f	60	83
7	H	Me	Br	5a	180	85
8	4-NO$_2$	Me	Br	5b	120	92
9	4-Cl	Me	Br	5c	120	90
10	4-CN	Me	Br	5g	90	90
11	4-OMe	Me	Br	5d	240	70
12	H	Bu^n	I	5h	20	95
13	4-NO$_2$	Bu^n	I	5i	20	95
14	4-Cl	Bu^n	I	5j	25	92
15	4-OMe	Bu^n	I	5k	30	90
16	4-Me	Bu^n	I	5l	30	95
17	2-Thiophene	Bu^n	I	5m	60	80
18	H	Bu^n	Br	5h	120	80
19	4-NO$_2$	Bu^n	Br	5i	120	92
20	4-OMe	Bu^n	Br	5k	160	75
21	H	Me	Cl	5a	5h/24h	10/10
22	4-CHO	Bu^n	Cl	5n	7h/24h	30/30
23	4-NH$_2$	Bu^n	Cl	5o	7h/24h	10/10

corresponding iodo analogues towards the Heck–Mizoroki reaction (Table 4, entries 7–11).

Moreover, as a comparative study, the scope of this catalytic system was examined with *n*-butyl acrylate as substrate. Interestingly, the reactions of *n*-butyl acrylate proceeded in shorter reaction times with excellent yields, which are due to more activity of *n*-butyl acrylate against methyl acrylate (Table 4, entries 12–20). Also, aryl chlorides such as chlorobenzene, 4-chlorobenzaldehyde and 4-chloroaniline were chosen as the challenging substrates. However, the catalytic system was less effective in this regard and even prolonged reaction time was required to obtain the reasonable yields of the desired product (Table 4, entries 21–23).

3.3 Heterogeneity Tests

In order to evaluate catalytic activity of the prepared ZrO₂@AEPH₂-PPh₂-Pd(0) as a heterogeneous nanocatalyst, a hot filtration test was performed in the Suzuki–Miyaura coupling reaction of iodobenzene with phenylboronic acid. Along this line, the nanocatalyst was separated from the reaction mixture by filtration after 5 min and the determined conversion was 35%. Afterwards, the filtrate allowed to react for further 3 h. The thin layer chromatography showed that the reaction did not proceed upon the removal of the solid nanocatalyst. Also, in a separated experiment, a hot-filtration test was performed in the Heck-Mizoroki coupling reaction of iodobenzene with methyl acrylate and the same result was obtained from this reaction. These findings provide direct evidence for no leaching of palladium takes place during the reaction and confirming the truly heterogeneous nature of the ZrO₂@AEPH₂-PPh₂-Pd(0) nanocatalyst.

In addition, to further determine any leaching of palladium in the reaction mixture and to show that ZrO₂@ AEPH₂-PPh₂-Pd(0) is a heterogeneous nanocatalyst, we conducted a poisoning test with Hg(0) for the Suzuki–Miyaura coupling reaction of iodobenzene with phenylboronic acid in the presence of a large excess of Hg(0) (Hg/Pd, 300:1) under the optimized reaction conditions. In this experiment, the desired biphenyl product was obtained in excellent yield. This result indicates that the catalytic activity of nanocatalyst comes from the leached out Pd [79].

3.4 Reusability of the ZrO₂@AEPH₂-PPh₂-Pd(0) Nanocatalyst

The reusability of the catalyst is a very important issue, especially for commercial and industrial applications. So, in relevance with this, we studied the recyclability of ZrO₂@ AEPH₂-PPh₂-Pd(0) nanocatalyst for a Suzuki–Miyaura

reaction of iodobenzene with phenylboronic acid, under the optimized reaction conditions (Fig. 7). Upon completion of the reaction, the nanocatalyst was recovered by centrifuging and washed with ethyl acetate (3×10 mL) to remove the organic products. Then, the recycled catalyst was dried at 100 °C under vacuum for 24 h and used for the next run of the model reaction. Figure 7 depicts the results obtained after six reused cycles. As can be seen in Fig. 7, no significant loss of the nanocatalyst activity is observed, which demonstrates the practical recyclability of the synthesized nanocatalyst. Since the phosphine ligands are highly efficient stabilizers for Pd nanoparticles [58, 65, 80, 81], the high catalytic performance of the aforementioned catalytic system would possibly relate to the strong interaction of Pd nanoparticles with phosphorous atoms on chlorodiphenylphosphine.

The Pd content of the freshly prepared ZrO₂@AEPH₂-PPh₂-Pd(0) nanocatalyst which was obtained by inductively coupled plasma (ICP) was 0.43 mmol of Pd per 1.00 g of catalyst, while ICP analysis of 6th reused nanocatalyst displayed that the recovered nanocatalyst contains 0.41 mmol of Pd per 1.00 g of catalyst. However, application of a hot filtration test followed by inductively coupled plasma optical emission spectrometer (ICP-OES) analysis of the liquid phase of the reaction mixtures for each cycle showed that very little Pd was present in the solution (less than 1 ppm) and the solid-free filtrate did not promote the reaction any further. So, it can be concluded that the small amount of leached Pd could not be responsible for most of the activity and the catalysis was due to heterogeneous sites.

To gain a deep insight on the structure stability of ZrO₂@AEPH₂-PPh₂-pd(0) after six runs, the recovered
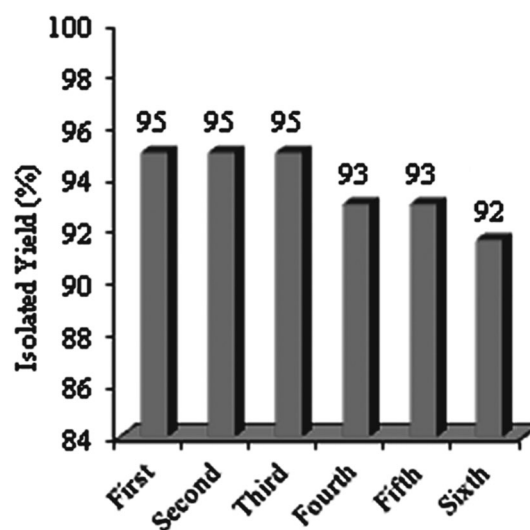

Fig. 7 The Suzuki–Miyaura reaction of iodobenzene with phenylboronic acid in the presence of reused ZrO₂@AEPH₂-PPh₂-Pd(0) nanocatalyst

nanocatalyst was characterized by XRD, XPS, SEM and TEM techniques. As presented in Fig. 2c, the XRD pattern of catalyst after six runs showed no considerable broadening or shifting of peaks when compared with the XRD pattern of the fresh catalyst. Furthermore, the XPS spectrum of the 6th recycled catalyst clearly showed the presence of peaks at 335.4 eV and 340.7, corresponding to $3d_{5/2}$ and $3d_{3/2}$ for Pd(0) species, respectively (Fig. 3b). These results suggested that the oxidation state of the immobilized Pd did not change after repeated reactions. Also, comparison of SEM and TEM images of sixth reused nanocatalyst (Fig. 4c, d, g, h) with the fresh ones (Fig. 4a, b, e, f) indicated that the morphology and structure of ZrO_2@AEPH$_2$-PPh$_2$-pd(0) remained intact after six recoveries. As shown in Fig. 4g, h, due to the slightly agglomeration of ZrO_2 nanoparticles, no obvious particle of Pd species can be found in the structure of nanocatalyst. In spite of this, obtained results from various characterization analysis of the reused nanocatalyst revealed that the recovered ZrO_2@AEPH$_2$-PPh$_2$-Pd(0) had not significantly lost its activity after six cycles.

4 Conclusion

In summary, ZrO_2@AEPH$_2$-PPh$_2$-Pd(0) as a new and efficient heterogeneous nanocatalyst was synthesized and characterized by FT-IR, XRD, XPS, SEM, EDS, TEM, TGA and ICP techniques. Characterization results showed that ZrO_2@AEPH$_2$-PPh$_2$-Pd(0) had spherical morphology with an average size ranging of 10–40 nm. The catalytic activity of this new aminophosphine nanocatalyst has been proved for Suzuki–Miyaura and Heck–Mizoroki cross-coupling reactions. A series of aryl iodides and bromides were coupled with phenylboronic acid and alkyl acrylates to produce the corresponding products in short reaction times and excellent yields. Applying green solvents such as H_2O and PEG 600 are also the predominant features supporting this approach in a movement towards the green chemistry. Moreover, this catalyst can be easily recovered and reused for at least six cycles without deterioration in catalytic activity.

References

1. Johannes GV (2001) Can J Chem 79:1086–1092
2. Leroux F (2004) ChemBioChem 5:644–649
3. Lightowler S, Hird M (2005) Chem Mater 17:5538–5549
4. Kozlowski MC, Morgan BJ, Linton EC (2009) Chem Soc Rev 38:3193–3207
5. Ogata A, Furukawa C, Sakurai K, Iba H, Kitade Y, Ueno Y (2010) Bioorg Med Chem Lett 20:7299–7302
6. Maitlis PM, Haynes A (2006) Metal-catalysis in industrial organic processes. RSC Publishing, Cambridge
7. Tappe FMJ, Trepohl VT, Oestreich M (2010) Synthesis 2010:3037–3062
8. Hiyama T, Diederich F, Stang PJ (1998) Metal-catalyzed cross-coupling reactions. Wiley-VCH, Weinheim
9. Ojima I (2000) Catalytic asymmetric synthesis. Wiley-VCH, New York
10. Miyaura N, Yamada K, Suzuki A (1979) Tetrahedron Lett 20:3437–3440
11. Heck RF, Nolley JP (1972) J Org Chem 37:2320–2322
12. Dieck HA, Heck RF (1974) J Am Chem Soc 96:1133–1136
13. Larhed M, Hallberg A, Negishi E (2002) Handbook of organo-palladium chemistry for organic synthesis. Wiley, New York
14. Beletskaya IP, Cheprakov AV (2000) Chem Rev 100:3009–3066
15. Tao L, Xie Y, Deng C, Li J (2009) Chin J Chem 27:1365–1373
16. Chanjuan X, Yongwei W, Xiaoyu Y (2008) J Organomet Chem 693:3842–3846
17. Koji S, Ryouta T, Tsukasa N, Hisashi F (2008) Angew Chem Int Ed 47:6917–6919
18. Yan R, Xu JX, Zhang YY, Wang D, Zhang MC, Zhang WQ (2012) Chem Eng J 200:559–568
19. Al-Hashimi M, Sullivan AC, Wilson JRH (2007) J Mol Catal A Chem 273:298–302
20. Bohrsch V, Hackenberger CPR (2010) ChemCatChem 2:243–245
21. Yang F, Li YF, Liu T, Xu K, Zhang LQ, Xu CM, Gao JS (2013) Chem Eng J 226:52–58
22. Moussa S, Siamaki AR, Gupton BF, Samy El-Shall M (2012) ACS Catal 2:145–154
23. Rana S, Maddila S, Yalagala K, Jonnalagadda SB (2015) Appl Catal A 505:539–547
24. Okumura K, Tomiyama T, Okuda S, Yoshida H, Niwa M (2010) J Catal 273:156–166
25. Shylesh S, Wang L, Thiel WR (2010) Adv Synth Catal 352:425–432
26. Beygzadeh M, Alizadeh A, Khodaei MM, Kordestani D (2013) Catal Commun 32:86–91
27. Zhang YY, Zhang MC, Zhang X, Wang XH, Zhang WQ (2013) Chem Eng J 215:96–104
28. Proch S, Mei Y, Villanueva JMR, Lu Y, Karpov A, Ballauff M, Kempe R (2008) Adv Synth Catal 350:493–500
29. Ramarao C, Ley SV, Smith SC, Shirley IM, DeAleida N (2002) Chem Commun 10:1132–1133
30. Ahn JM, Wentworth P, Janda KD (2003) Chem Commun 4:490–491
31. Uozumi Y, Yamada YMA, Beppu T, Fukuyama N, Ueno M, Kitamori T (2006) J Am Chem Soc 128:15994–15995
32. Biffis A, Zecca M, Basato M (2001) J Mol Catal A Chem 173:249–274
33. Astruc D, Lu F, Aranzaes JR (2005) Angew Chem Int Ed 44:7852–7872
34. Stevens PD, Fan JD, Gardinmalla HMR, Yen M (2005) Org Lett 7:2085–2088
35. Barder TE, Walker SD, Martinelli JR, Buchwald SL (2005) J Am Chem Soc 127:4685–4696
36. Falvello LR, Ginés JC, Carbó JJ, Lledos A, Navarro R, Soler T, Urriolabeitia EP (2006) Inorg Chem 45:6803–6815
37. Yan X, Liu Y, Xi C (2008) Appl Organomet Chem 22:341–345
38. Phan NTS, VanderSluys M, Jones CW (2006) Adv Synth Catal 348:609–679

39. Trzeciak AM, Ziółkowski J (2005) J Coord Chem Rev 249:2308–2322
40. Trzeciak AM, Ziółkowski J (2007) J Coord Chem Rev 251:1281–1293
41. Liu Sh, Han MY (2010) Chem Asian J 5:36–45
42. Lu J, Zang JB, Shan SX, Huang H, Wang YH (2008) Nano Lett 8:4070–4074
43. Luo X, Morrin A, Killard AJ, Smyth MR (2006) Electroanalysis 18:319–326
44. Steiner SA, Baumann ThF, Bayer BC, Blume R, Worsley MA, MoberlyChan WJ, Shaw EL, Schlogl R, Hart AJ, Hofmann S, Wardle BL (2009) J Am Chem Soc 131:12144–12154
45. Gawande MB, Shelke SN, Branco PS, Rathi A, Pandey RK (2012) Appl Organomet Chem 26:395–400
46. Gawande MB, Branco PS, Parghi K, Shrikhande JJ, Pandey RK, Ghumman CAA, Bundaleski N, Teodoro OMND, Jayaram RV (2011) Catal Sci Technol 1:1653–1664
47. Gawande MB, Rathi AK, Branco PS, Potewar TM, Velhinho A, Nogueira ID, Tolstogouzov A, Ghumman CAA, Teodoro OMND (2013) RSC Adv 3:3611–3617
48. Liu H, Cheung P, Iglesia E (2003) J Phys Chem B 107:4118–4127
49. Xu X, Wang X (2009) Nano Res 2:891–902
50. Nakka L, Molinari JE, Wachs IE (2009) J Am Chem Soc 131:15544–15554
51. Tomishig K, Ikeda Y, Sakaihori T, Fujimoto K (2000) J Catal 192:355–362
52. Li W, Huang H, Li H, Zhang W, Liu H (2008) Langmuir 24:8358–8366
53. Wang R, Crozier PA, Sharma R, Adams JB (2008) Nano Lett 8:962–967
54. Monopoli A, Nacci A, Calo V, Ciminale F, Cotugno P, Mangone A, Giannossa LC, Azzone P, Cioffi N (2010) Molecules 15:4511–4525
55. Zarghani M, Akhlaghinia B (2016) Bull Chem Soc Jpn. doi:10.1246/bcsj.20160163
56. Jafarpour M, Rezapour E, Ghahramaninezhad M, Rezaeifard A (2014) New J Chem 38:676–682
57. Lomoschitz ChJ, Feichtenschlager B, Moszner N, Puchberger M, Muller K, Abele M, Kickelbickn G (2011) Langmuir 27:3534–3540
58. Du Q, Zhang W, Ma H, Zheng J, Zhou B, Li Y (2012) Tetrahedron 68:3577–3584
59. Jayakumar S, Ananthapadmanabhan PV, Thiyagarajan TK, Perumal K, Mishra SC, Suresh G, Su LT, Tok AIY (2013) Mater Chem Phys 140:176–182
60. Kazemi F, Saberi A, Malek-Ahmadi S, Sohrabi S, Rezaie HR, Taheriri M (2011) Ceramics-Silikáty 55:26–30
61. Veisi H, Gholami J, Ueda H, Mohammadi P, Noroozi M (2015) J Mol Catal A Chem 396:216–223
62. Farjadian F, Hosseini M, Ghasemi S, Tamami B (2015) RSC Adv 5:79976–79987
63. Ozawa F, Kubo A, Hayashi T (1992) Chem Lett 11:2177–2180
64. Iranpoor N, Firouzabadi H, Azadi R (2007) Eur J Org Chem 2007:2197–2201
65. Ebrahimzadeh F, Tamami B (2015) Phosphorus Sulfur Silicon Relat Elem 190:144–157
66. Iranpoor N, Firouzabadi H, Motevalli S, Talebi M (2012) J Organomet Chem 708:118–124
67. Ukisu Y (2015) Reac Kinet Mech Cat 114:385–394
68. Shen C, Wang YJ, Xu JH, Wang K, Luo GS (2012) Langmuir 28:7519–7527
69. Adlim M, Abu Bakar M, Liew KY, Ismail J (2004) J Mol Catal A Chem 212:141–149
70. Wang X, Lu G, Guo Y, Qiao D, Zhang Z, Guo Y, Li C (2008) Chin J Catal 29:1043–1050
71. Razavi N, Akhlaghinia B (2015) RSC Adv 5:12372–12381
72. Ghodsinia SSE, Akhlaghinia B (2015) RSC Adv 5:49849–49860
73. Zarei Z, Akhlaghinia B (2015) Chem Pap 69:1421–1437
74. Zarghani M, Akhlaghinia B (2015) Appl Organometal Chem 29:683–689
75. Zarghani M, Akhlaghinia B (2016) RSC Adv 6:31850–31860
76. Razavi N, Akhlaghinia B (2016) New J Chem 40:447–457
77. Jahanshahi R, Akhlaghinia B (2016) RSC Adv 6:29210–29219
78. Ghodsinia SSE, Akhlaghinia B (2016) RSC Adv 6:63613–63623
79. Yu K, Sommer W, Richardson JM, Weck M, Jones CW (2005) Adv Synth Catal 347:161–171
80. Khalafi-Nezhad A, Panahi F (2013) J organomet chem 741:7–14
81. Panahi F, Zarnaghash N, Khalafi–Nezhad A (2016) New J Chem 40:1250–1255